Numerical simulations of the QAB and Langavant semi-adiabatic tests : Analysis and comparison with an experimental measurement campaign

Matthieu Briffaut, Georges Nahas, Farid Benboudjema, Jean Michel Torrenti

Numerical simulations of the QAB and Langavant semi-adiabatic tests: Analysis and comparison with an experimental measurement campaign

Matthieu BRIFFAUT*
Georges NAHAS
LMT Cachan/ENS Cachan/CNRS UMR8535/ UPMC/PRES UniverSud Paris, Cachan, France
Institut de radioprotection et de sûreté nucléaire, Fontenay-aux-Roses, France

Farid BENBOUDJEMA
LMT Cachan/ENS Cachan/CNRS UMR8535/ UPMC/PRES UniverSud Paris, Cachan, France

Jean-Michel TORRENTI
Université Paris-Est, Laboratoire central des Ponts et Chaussées, Paris, France

ABSTRACT

In this paper, experimental and numerical results on two types of semi-adiabatic tests have been compared. These types of tests are of particular interest since they are simple and straightforward to perform. However, analysis of these tests may still be difficult since several underlying assumptions need to be addressed. A numerical study has also been undertaken in order to validate or reject some of these assumptions, which are capable of leading to misleading results. Moreover, the effect of activation energy, which plays a key role in the prediction of hydration, has been studied. Results indicate the need for a dual study to both identify and predict early-age behavior of massive concrete structures.

Simulations numériques des essais semi-adiabatiques QAB et Langavant : analyse et comparaison à des mesures expérimentales

RÉSUMÉ

Dans cette étude, nous avons comparé les résultats de simulations numériques et de mesure expérimentale concernant deux types de calorimètre semi-adiabatique. Ces essais sont particulièrement intéressants car simples et faciles à mettre en œuvre. Néanmoins, leur analyse peut s'avérer délicate car elle s'appuie sur des hypothèses fortes que nous avons voulu vérifier par des calculs aux éléments finis. Cette étude a donc permis d'établir la validité de ces hypothèses et de montrer que certaines simplifications du protocole aboutissent à une erreur importante sur les résultats. D'autre part, nous avons étudié l'influence d'un paramètre clé de la modélisation de l'hydratation d'un matériau cimentaire - l'énergie d'activation - pour mettre en exergue le fait que sa détermination devait se faire en même temps que l'affinité chimique.

***Corresponding author:**
Matthieu BRIFFAUT
briffaut@lmt.ens-cachan.fr

INTRODUCTION

In order to determine the heat release or hydration degree evolution in concrete elements, semi-adiabatic testing is especially attractive given that these tests are simple and easy to implement in comparison with an adiabatic test. Semi-adiabatic tests prove to be less expensive and offer the potential for in situ applications. During so-called adiabatic testing, heat losses from the sample towards the external environment are in fact being compensated by holding the sample environment at the same temperature as the sample itself. This step therefore requires a servo-controlled heat source; let's cite for example research conducted by Suzuki **[20]**, Coole **[7]**, Bamforth **[3]** and Costa **[9]** (a more exhaustive review of the various adiabatic calorimeters used can be found in Springerschmidt **[19]**). In so-called semi-adiabatic tests, heat losses are simply limited by thermal insulation. Semi-adiabatic calorimeters can be divided into two categories depending on the type

of thermal insulation (high-vacuum vs. insulating material); we have thus decided to study two calorimetric tests, one for each insulation type, i.e.:

• the standardized Langavant bottle test **[11]**;

• the QAB test developed at the LCPC Laboratory **[1]**.

From a classical perspective, device calibration is necessary to interpret semi-adiabatic test results (to determine both the loss coefficient α and corresponding heat capacity μ). In knowing the heat capacity of the concrete specimen, along with the change in both concrete temperature $T_{concrete}$ and external temperature T_{ext}, the quantity of heat released q during hydration can be written as follows:

$$\begin{aligned} q(t_{sa}) &= C_{béton}\left(T_{ad}(t_{sa}) - T_{ad}(t_{sa}=0)\right) \\ &= C_{tot}\left(T_{béton}(t_{sa}) - T_{béton}(t_{sa}=0)\right) + \int_0^{t_{sa}} \left(a + b\theta(t)\right)\theta(t)\,dt \end{aligned} \quad (1)$$

where: $C_{concrete}$ is the heat capacity of concrete alone [J.°C^{-1}]; $C_{tot} = C_{concrete} + \mu$ is the total heat capacity (concrete + calorimeter); a[W] and b [W·°C^{-1}] are the calorimeter heat loss coefficients (such that $\alpha = a + b\theta$); t_{sa} [s] is the real time of the semi-adiabatic test; $\theta = T_{concrete} - T_{ext}$ is the heating level [°C]; and T_{ad} is the theoretical concrete temperature under adiabatic conditions [°C].

Since the hydration reaction is exothermic, the time parameter must be corrected for comparison with a reference temperature scale (e.g. the virtual temperature T_{ad} that would be generated during an adiabatic test). The rate of heat release during an adiabatic test will be faster, and the transition between the time scale associated with the semi-adiabatic test t_{sa} and the adiabatic test time scale t_{ad} can be derived from the following relation (in assuming that thermo-activation is governed by Arrhenius' Law **[12, 16]**):

$$t_{ad} = \int_0^{t_{sa}} e^{\frac{E_a}{R}\left[\frac{1}{(273+T_{ad}(t))} - \frac{1}{(273+T_{béton}(t))}\right]} dt \quad (2)$$

where E_a is the cement activation energy [J·mol^{-1}] and R the perfect gas constant [8.314 J·mol^{-1}·K^{-1}].

Based on these results, it becomes possible to determine the quantity of heat released during hydration, regardless of the temperature history, as well as changes in the degree of hydration (based on the thermochemistry, *see* for example **[21]**). The latent heat of hydration L [J·m^{-3} C^{-1}] and normalized chemical affinity $\tilde{A}(\xi)$ [s^{-1}] (material parameters required as model input, *see* below) can both be deduced based on the previous corrections:

$$L = C\frac{\left(T_\infty^{ad} - T_0^{ad}\right)}{\xi_\infty} \quad \text{and} \quad \tilde{A}(\xi) = \xi_\infty \frac{dT^{ad}/dt}{T_\infty^{ad} - T_0^{ad}} \exp\left(\frac{E_a}{RT(t)}\right) \quad (3)$$

where ξ is the degree of hydration, ξ_∞ the final degree of hydration, T the temperature [K], C the volumetric heat capacity [J·m^{-3} K^{-1}], T_∞^{ad} the final adiabatic temperature (i.e. $\xi = \xi_\infty$), and lastly T_0^{ad} is the initial adiabatic temperature (*i.e.* $\xi = 0$).

On the other hand, this analysis introduces several disadvantages as well, namely:

• The cement activation energy needs to be known; this value may be estimated from a number of cement characteristics **[17]**. Several experimental methods are available for this characterization step (e.g. **[10]**), yet activation energy depends on temperature and the value obtained differs from one method employed to the next. A whole range of hydration reactions actually occurs, yielding various pairs of activation energy values and kinetics.

• Semi-adiabatic devices are calibrated in the steady state, whereas the test is conducted in a transient state.

For this reason, the semi-adiabatic devices were numerically simulated in order not only to verify our capacity to numerically reproduce testing campaigns from experimental data, but also to assert that in the transient state, calorimeter loss coefficients continue to be expressed in the form: $\alpha(\theta) = a + b\theta$.

Moreover, during execution of a Langavant type test, it might be beneficial to measure air temperature above the mortar sample by assuming that the entire calorimeter cell remains at the same temperature (so as to directly reuse the temperature probe). It is important to first verify experimentally and numerically whether this hypothesis is justifiable and then quantify the error produced on final results (changes in the degree of hydration as well as in the latent heat of hydration for concrete).

As a last step, we carried out a parametric study on the activation energy, for the purpose of interpreting semi-adiabatic test results, to determine the level of accuracy required for this value when performing, for example, temperature calculations on a solid concrete element.

MODELING OF A QAB TEST

The mesh and model employed

Mesh

In the QAB test, the study sample is cylindrical, whereas the calorimeter has a parallelepiped shape. As such, an axisymmetric model would be overly simplistic and, for reasons of symmetry, our approach entails a three-dimensional model that depicts one-quarter of the sample-calorimeter set-up (*see* **Fig. 1**).

Thermal model

The temperature change is derived by solving the heat equation, which includes heat released due to the hydration reaction, i.e.:

$$C\dot{T} = \nabla\left(k\nabla T\right) + L\dot{\xi} \qquad (4)$$

where k is the coefficient of thermal conduction [$W \cdot m^{-1} K^{-1}$]. This parameter, as well as the latent heat of hydration and volumetric heat capacity, can be assumed constant over time **[15, 23]**. The

Figure 1
Mesh of one-quarter of the QAB test

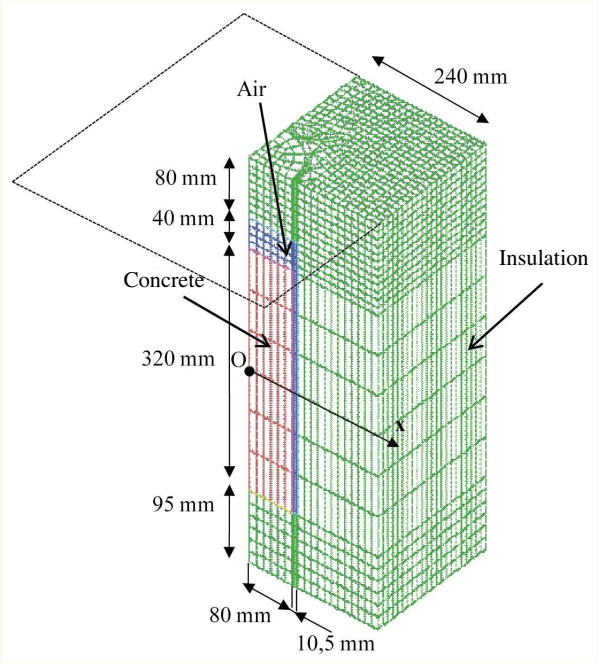

effects of both convection and radiation in air inside the calorimeter are incorporated into these conduction coefficients, which in turn simplifies the model (*see* **Table 1**, and **[13]**).

The next step calls for introducing an Arrhenius type relation, using the notation proposed by Ulm and Coussy **[21]** for thermo-activation:

$$\dot{\xi} = \tilde{A}(\xi)\exp\left(-\frac{E_a}{RT}\right) \quad (5)$$

In Equations **(4)** and **(5)**, the latent heat of hydration and normalized chemical affinity stem from analysis of a QAB test conducted at LCPC on a concrete whose mix design is representative of concretes used when building massive structures.

Boundary conditions are of the convective type. Heat flux φ can be written in the following form:

$$\varphi = h\left(T_s - T_{ext}\right)\mathbf{n} \quad (6)$$

where h is the convection exchange coefficient [W·m^{-2} K^{-1}], T_s the temperature at the calorimeter surface [K], T_{ext} the ambient temperature [K], and **n** the unit vector normal to the surface. Let's point out that parameter h also integrates radiation exchanges (which are linearized given the limited temperature variation range: *see the section* "Modeling of the Langavant test, *Thermal model*", and **[13]**). The value of this parameter at the free surface corresponds to the value proposed in Set of Rules ThK 77 (*see* **Table 1**).

The thermal parameters used herein are listed in **Table 1**; the heat capacity of the insulating material was identified based on the overall QAB heat capacity (as measured during the calibration step at 3,266 J·K^{-1}).

Table 1
Thermal parameters used for the QAB test numerical simulations.

	h [W·m^{-2} K^{-1}]	k[W·m^{-1} K^{-1}]	C[J·m^{-3} C^{-1}]	L[W·m^{-3}]	E_a/R [K]
Air		0.088(1)	1200		
Insulation		0.03	14 680		
Concrete		1.7	2.4×10^6	154.7×10^6	5 500
Soil surface	0.6 [6]				
Free surfaces	9(2)				

(1) Thermal conductivity of the air equals 0.0257 W·m–1 K^{-1} at 20°C. The (highest) value listed in this table takes account of both the convective and radiative exchanges **[13]**.
(2) Value proposed for a vertical surface by the ThK 77 Rules, in accounting for convective and radiative exchanges.

Analysis of these results

The output presented in this study was derived by applying the finite element computation code Cast3m, developed by France's Atomic Energy Commission (CEA). Simulation results in terms of temperature evolutions in the QAB are shown in **Figure 2**.

In this figure, a strong level of agreement is observed between numerical results and QAB test findings regarding both kinetics and maximum obtained value. Two points need to be made here: first, the modeling process was simplified (non-inclusion of thermal bridges at the level of the cap and when passing the thermocouple, no taking in account the rigid calorimeter shell, a geometry modeled as regular even though in reality such is not the case) and second, temperature probe accuracy is on the order of 1 degree.

According to **Figure 3**, temperature profiles over time reveal a temperature threshold for abscissa values below 0.08 m (*i.e.* inside the concrete). This observation indicates that the temperature gradient within the concrete is small (hence, precise temperature probe placement is unnecessary). Such a conclusion can also be drawn from **Figure 4**, where temperature iso-values at various times have been displayed.

Figure 2
Temperature vs. time at Point O (located at the core of the concrete specimen, see Fig. 1)

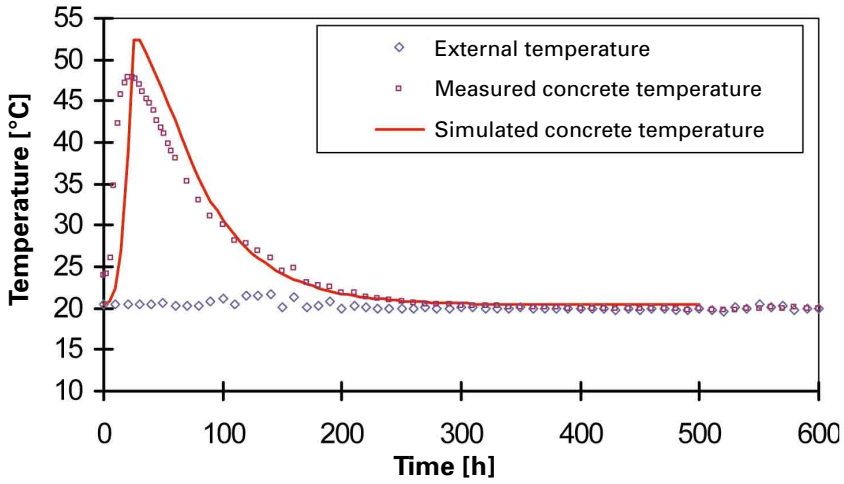

Figure 3
Modeled depiction of the spatial evolution of temperature in the QAB test vs. abscissa (see Fig. 1) at various points in time

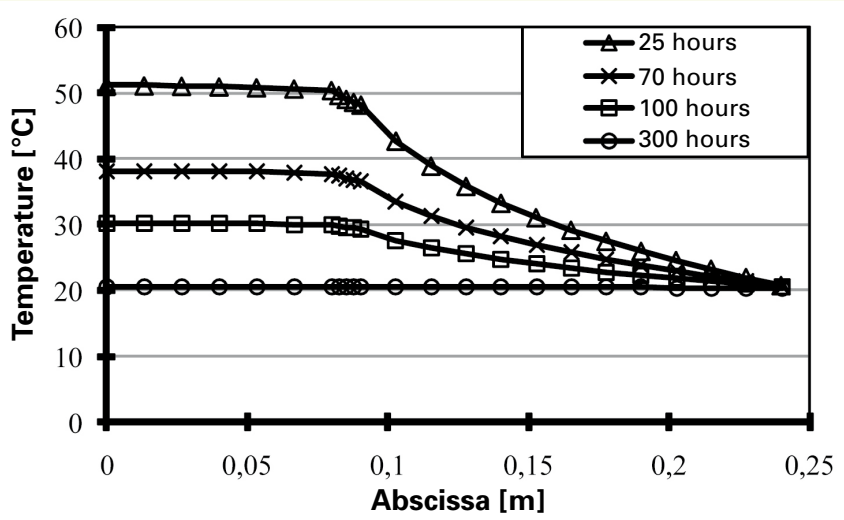

Figure 5 compares the transient state results (at 25 hours) with those at steady state (concrete temperature is set at a uniform 51.1°C, which corresponds to the temperature at the specimen core at a time of 25 hours, while the external temperature is set at 20.2°C). Let's note that the steady state is reached very quickly (after approx. 10 hours). The 2 curves are seen to nearly overlap, which conforms with the previous result since the insulating material possesses low thermal conductivity, yet at the same time its volumetric heat capacity is also low, thus making its thermal diffusion coefficient (i.e. thermal conductivity divided by volumetric heat capacity) high (on the same order of magnitude as that of concrete). This finding serves to validate the steady-state calibration method.

The correction proposed in **Equation (1)** assumes that temperature in the insulating material is homogeneous and equal to the concrete value temperature. **Figures 3 and 4** demonstrate that insulation temperature is in fact not uniform. To identify the limitations of this approximation, **Figure 6** compares the quantity $q_{t1} = \int_0^t C_{iso}\left(T_{iso}(t) - T_{iso}(0)\right) dV_{iso}$, where C_{iso} = 14 680 J m^{-3} K^{-1} (*see* **Table 1**) is the volumetric heat capacity of the insulating material, with the quantity $q_{i2} = C_{iso}(T_{béton}(t) - (T_{béton}(0))$, where C_{iso} = 3266 J K^{-1} is the total heat capacity of the insulating material (in assuming that concrete temperature is uniform and equal to its value at the specimen core $T_{concrete}$, which

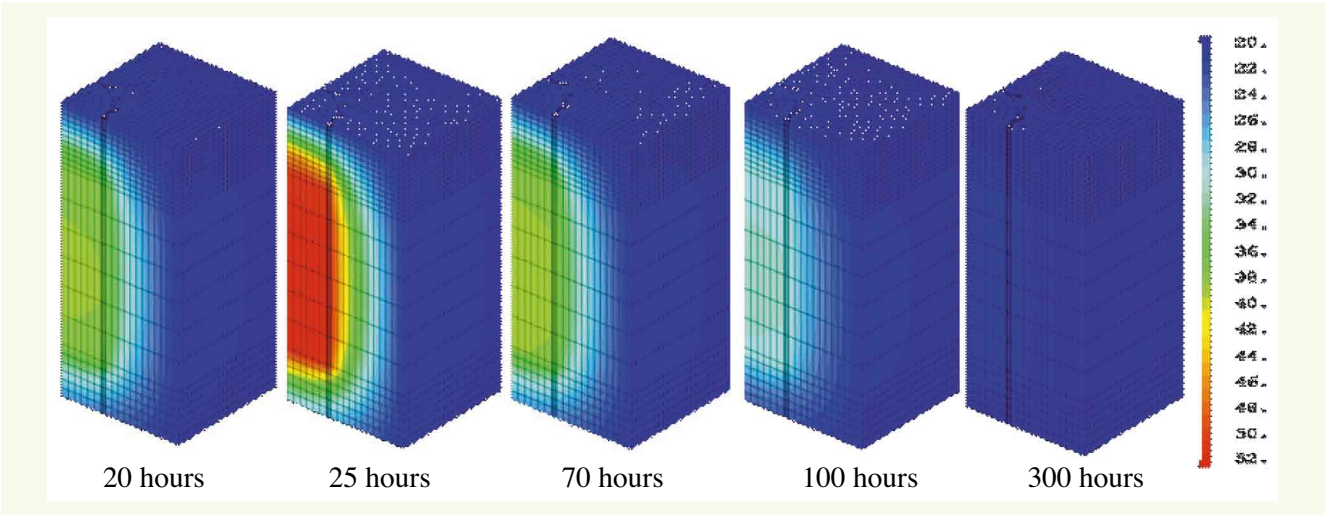

Figure 4
Temperature iso-values at various times in the QAB test

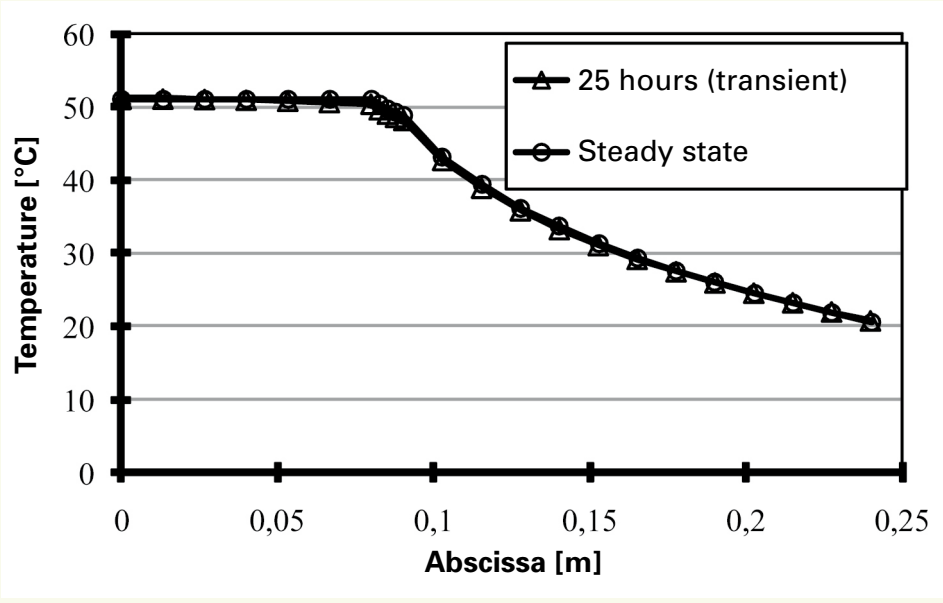

Figure 5
Spatial evolution of temperature in the QAB test vs. abscissa (see Fig. 1) at 25 hours and in the steady state (with concrete temperature held at a constant 51.1°C)

proves to be a realistic assumption – *see* **Fig. 3**). **Figure 6a** shows a major deviation between these 2 quantities (a nearly constant ratio of 135 over the time interval between q_{i2} and q_{i1}), which seems to contradict the correction **Equation (1)**.

It should be pointed out however that the total heat capacity of concrete (C_{tot}) equals 15 440 J·K^{-1}, which is roughly 5 times greater than that of the insulation (3 266 J·K^{-1}). The total heat capacity of air is negligible (3.4 J·K^{-1}). We also compared therefore the quantities $q_{t1} = \int_0^t C_{iso}\left(T_{iso}(t) - T_{iso}(0)\right)\mathrm{d}V_{iso} + C_{bét}\left(T_{bét}(t) - T_{bét}(0)\right)\mathrm{d}V_{bét}$ and $q_{t2} = C_{tot}(T_{béton}(t) - (T_{béton}(0))$ (corresponding to the correction proposed in **Equation (1)**). **Figure 6b** underscores the limited role played by insulation in the calculation of accumulated heat (yet not in the calculation of heat losses, given that these losses are reduced via coefficients *a* and *b*). It can be remarked that a value of approximately $\int_0^t C_{bét}\left(T_{bét}(t) - T_{bét}(0)\right)\mathrm{d}V_{bét} \approx 680 \int_0^t C_{iso}\left(T_{iso}(t) - T_{iso}(0)\right)\mathrm{d}V_{iso}$ is maintained throughout the duration of the test, meaning that **Equation (1)** can be validly used.

Figure 7 confirms that a law of the type $y = \alpha(\theta)\cdot\theta$ (with $\alpha(\theta) = a + b\theta$, where *b* is small in comparison with *a*) for the heat loss calculation is indeed acceptable. The numerical and experimental

Figure 6a
Evolution in accumulated heat inside the insulating material q_{i1}. Comparison with the value proposed in the QAB correction (q_{i2})

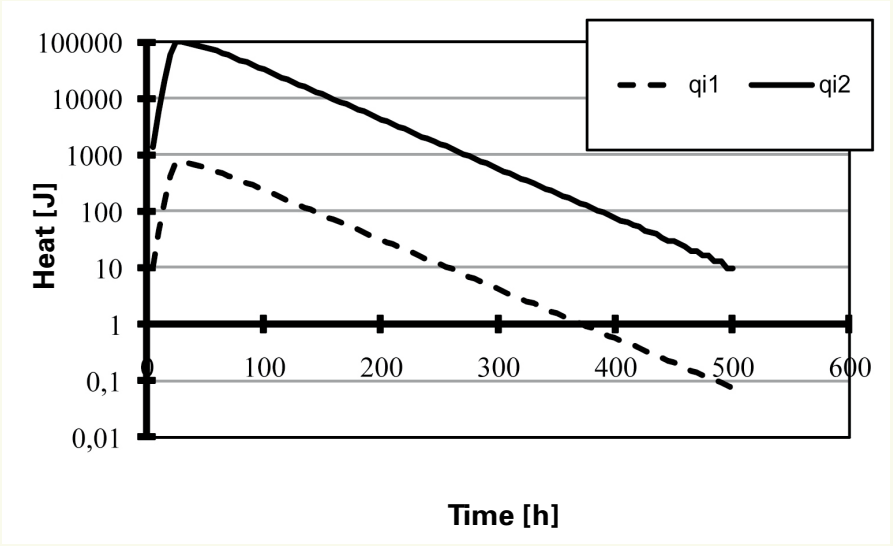

Figure 6b
Evolution in accumulated heat inside the caisson set-up (concrete, air + insulation = q_{t1}): Comparison with the value proposed in the QAB correction (q_{t2})

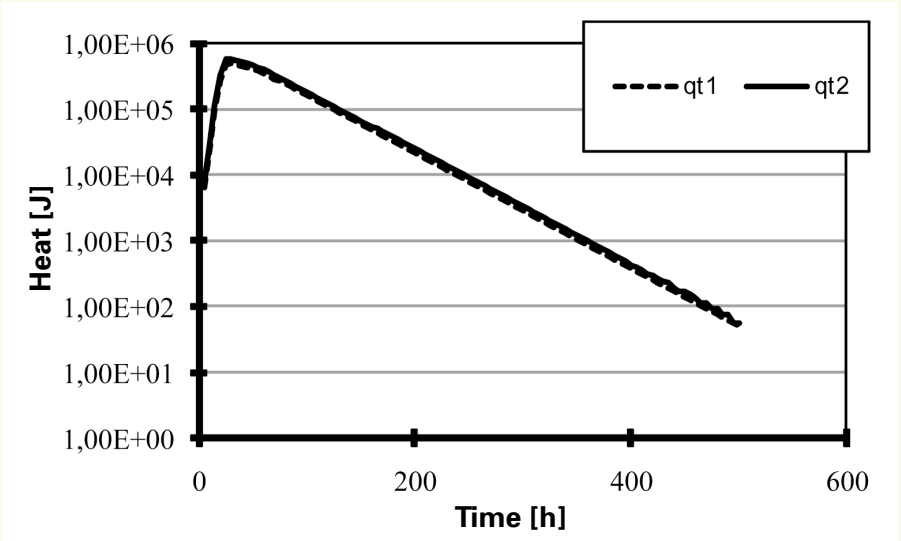

Figure 7
Evolution in heat losses vs. the difference (θ) between specimen temperature and external temperature

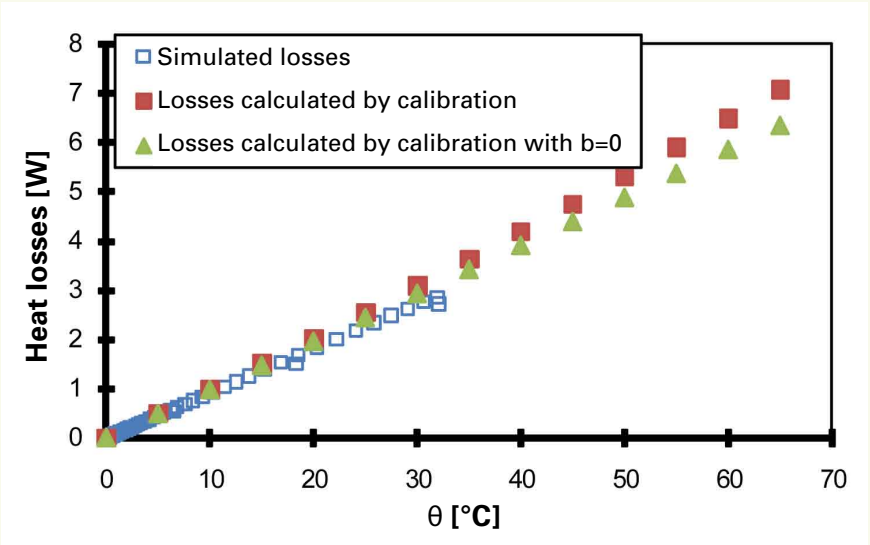

results relative to lost flux are similar, though slightly lower in our model output. This finding would explain the overestimation of maximum temperature throughout the test duration (**Fig. 2**), due therefore to an underestimation of heat losses.

Figure 7 also reveals that over a wide measurement range ($\Delta\theta = 40°C$, which covers the majority of cases), the coefficient *b* may be neglected due to its limited influence (this step however would lead to slightly altering the value of coefficient *a*). In essence, heat is transferred by means of first conduction then convection at the level of external surfaces. Radiation (which introduces non-linearity into the set of thermal transfer equations) only occurs in the small volume of air contained in the QAB and at the level of external surfaces (where the limited temperature variation justifies the step of linearizing radiation equations). **Figure 8** demonstrates that a significant proportion of heat flux is lost through the lateral surfaces.

Figure 8
Evolution of heat losses in the QAB via different directions

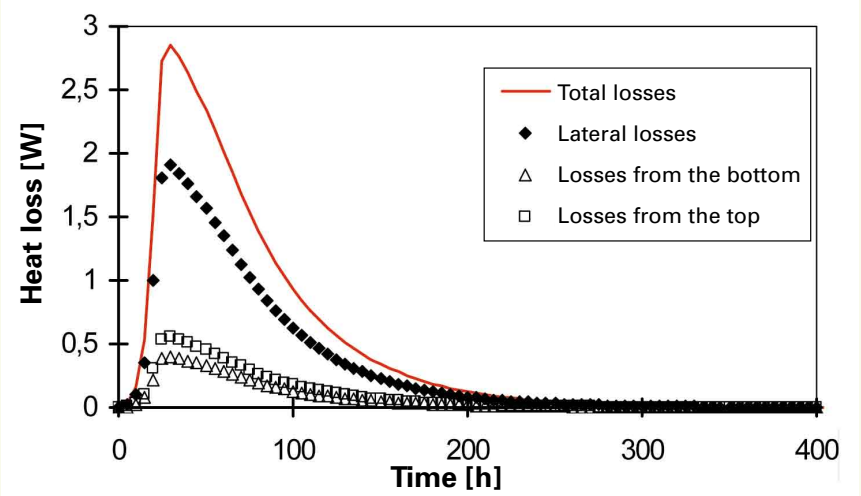

MODELING OF THE LANGAVANT TEST

Mesh and model introduced

› Mesh

As opposed to the QAB test, the calorimeter used as part of the Langavant test as well as the actual sample tested are both cylindrical, a condition that makes it possible to introduce an axisymmetric rotating mesh (**Fig. 9**).

› Thermal model

The primary difficulty encountered when modeling the Langavant test lies in modeling heat transfer within the vacuum (Dewar flask). To tackle this difficulty, we considered radiation as an equivalent conduction by means of linearizing the heat flux transmitted by radiation, in order to place it into the same form as a heat flux transmitted by conduction. The heat flux transmitted by radiation between two plates is written as follows:

$$\varphi = \varepsilon\sigma\left(T_{int}^4 - T_{ext}^4\right) \quad (7)$$

where ε is the surface emissivity [-], σ the Stefan-Boltzmann constant [$5.67 \times 10^{-8} W \cdot m^{-2} \cdot K^{-4}$], T_{int} the temperature of the first plate [K], and T_{ext} the temperature of the second plate [K].

The following form can also be used to express this relation:

$$\varphi = \varepsilon\sigma\left(T_{int} - T_{ext}\right)\left(T_{int}^3 + T_{int}^2 T_{ext} + T_{int} T_{ext}^2 + T_{ext}^3\right) \approx 4\varepsilon\sigma T_{moy}^3 \left(T_{int} - T_{ext}\right) = \frac{\lambda_{eq}}{e}\left(T_{int} - T_{ext}\right) \quad (8)$$

Figure 9
Axisymmetric mesh used in the Langavant test

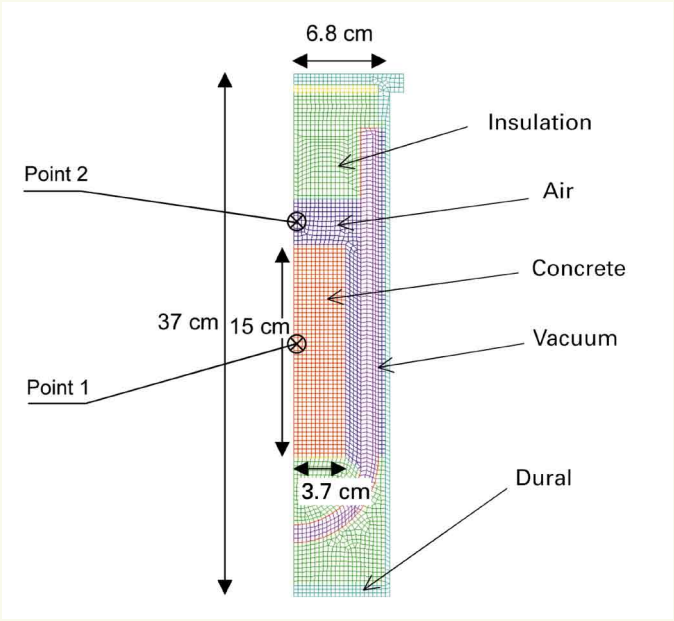

where $T_{ave} = (T_{ext} + T_{int})/2$, e is the Dewar flask thickness (m), and λ_{eq} the equivalent thermal conductivity [$W \cdot m^{-1} \cdot K^{-1}$].

This approximation, which has been used on a regular basis in the past **[13]**, is only valid provided the temperature difference $T_{int} - T_{ext}$ remains moderate, which is the case here.

Modeling the Langavant bottle test is equivalent to a conduction problem with a nonlinear conduction coefficient, which is dependent both on the temperature field at the "virtual" mesh of the vacuum and on convective boundary conditions. The model applied is thus identical to that developed in the section entitled: "Modeling of a QAB test, *Thermal model*".

The thermal parameter values introduced are listed in **Table 2** below.

Table 2
Thermal parameter values used in the Langavant test simulation.

	ε[-]	*h* [$W \cdot m^{-2} \cdot K^{-1}$]	*k* [$W \cdot m^{-1} \cdot K^{-1}$]	*C* [$J \cdot m^{-3} \cdot K^{-1}$]	*L* [$W \cdot m^{-3}$]	E_a/R [K]
Air			0.088	1200		
Insulating material			0.043	13000		
Equivalent concrete mortar			2	2.460×10^6	129.6×10^6	5,500
Dural			200	860		
Dewar flask wall	0.023					
Free surface		8				

Analysis of results

It needs to be emphasized that the samples tested in a Langavant-type calorimeter are not adequately sized to test concretes in a representative manner: this is a main reason behind LCPC's motivation to devise the QAB test. For their part, Schwartzentruber *et al.* **[18]** developed the concept of equivalent concrete mortar (ECM). The principle herein consists of replacing the granular fraction, with a diameter that exceeds 5 mm, by sand while maintaining the same granular specific surface area as the reference concrete. Initially intended for rheological studies, Schwartzentruber *et al.* **[18]** demonstrated that the representativeness of ECM with respect to the reference concrete was valid in calorimetric terms as well.

Furthermore, we conducted experimental and numerical tests by measuring and calculating the temperature at two distinct positions (one in the center of the ECM (1) the other in the middle of the air layer above the sample (2)). We selected these two measurement points since even though the standard prescribes making a recording at the level of Point 1 (in the mortar sample), it is physically advantageous to place the temperature probe at Point 2 in order to easily recover it upon completing each test. **Figure 10** shows the temperature vs. time inside the calorimeter at Points 1 and 2.

Results from this comparison are worthwhile for several reasons. First, a strong correlation is observed between simulation output and experimental findings, which sparks interest since the ECM thermochemical parameters (i.e. chemical affinity and latent heat of hydration) introduced into this simulation actually stem from the QAB test and not from a Langavant test. Accordingly, this study allows us to validate the hypothesis of ECM representativeness with respect to the reference concrete in calorimetric terms.

The second key result of this study is the significant temperature difference between Points 1 and 2, which serves to invalidate the hypothesis of constant temperature throughout the calorimeter cell. This difference will obviously influence calculation of the latent heat of hydration, and it can be debated whether the degree of hydration kinetics is affected by such a discrepancy. The kinetics of temperature evolution are in fact similar, and since the degree of hydration is determined by relating the evolution in adiabatic temperature to final adiabatic temperature, it is indeed possible that this difference does not alter normal changes in the degree of hydration. According to this logic however, thermo-activation (more pronounced at Point 1 than at Point 2) is not incorporated. By promoting the classical rationale of Langavant test interpretation (i.e. compensation of losses in order to obtain the adiabatic temperature, and time correction by means of thermo-activation), Figures **11** and **12** can be derived.

Figure 11 shows a significant difference in adiabatic temperature over time, ultimately leading to an error of approx. 22% on the latent heat of hydration calculation. The error committed on the degree of hydration **(Fig. 12)** is smaller yet not altogether negligible since on average it amounts to 8%. It is necessary therefore to comply with Standard EN 196-8 and place the temperature probe at the core of the sample. This Standard also proposes containing the probe within a thermometer case, i.e. a hollow cylinder filled with oil, so as to ensure high conductivity, which also enables probe recovery upon test completion.

Figure 13 offers a comparison of losses obtained by both simulation and calorimeter calibration. The losses predicted by finite element calculation are less than those found due to calibration, yet a linear relation (of the type $y = \alpha \cdot (\theta)\theta$, where $\alpha(\theta) = a + b\theta$ and b is small in comparison with a) can still be identified.

Figure 10
Temperature vs. time (at Points 1 and 2) during a Langavant test

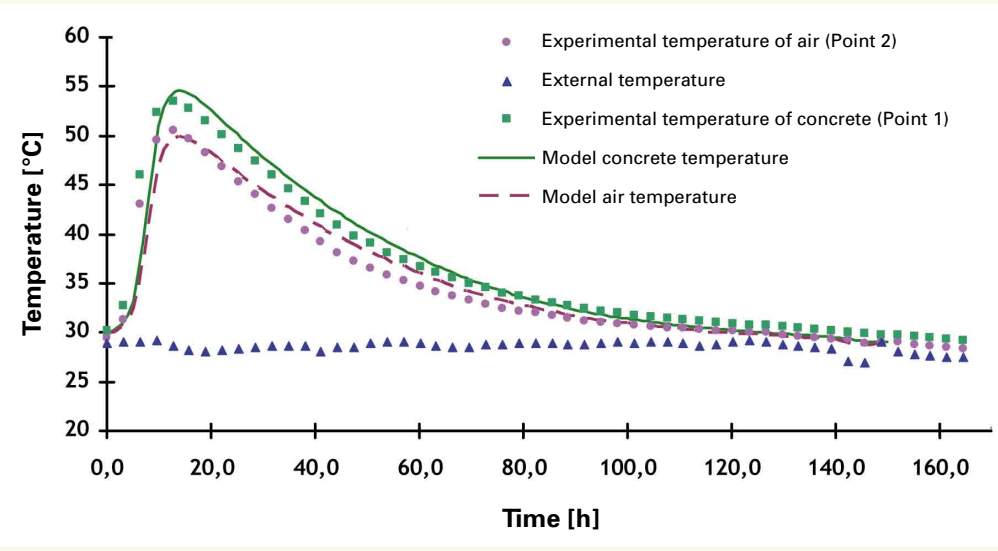

Figure 11
Evolution in adiabatic temperatures derived from temperatures measured at Points 1 and 2

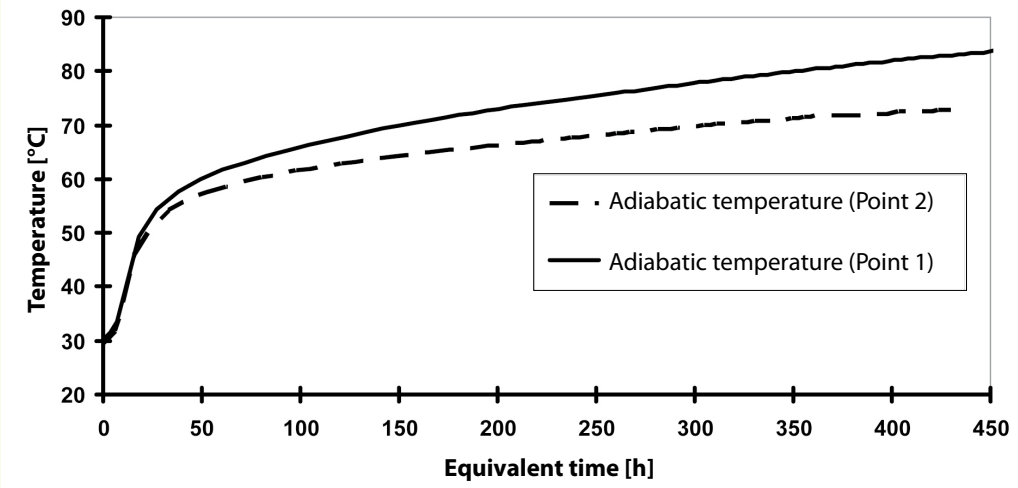

Figure 12
Evolution in degree of hydration stemming from temperatures measured at Points 1 and 2

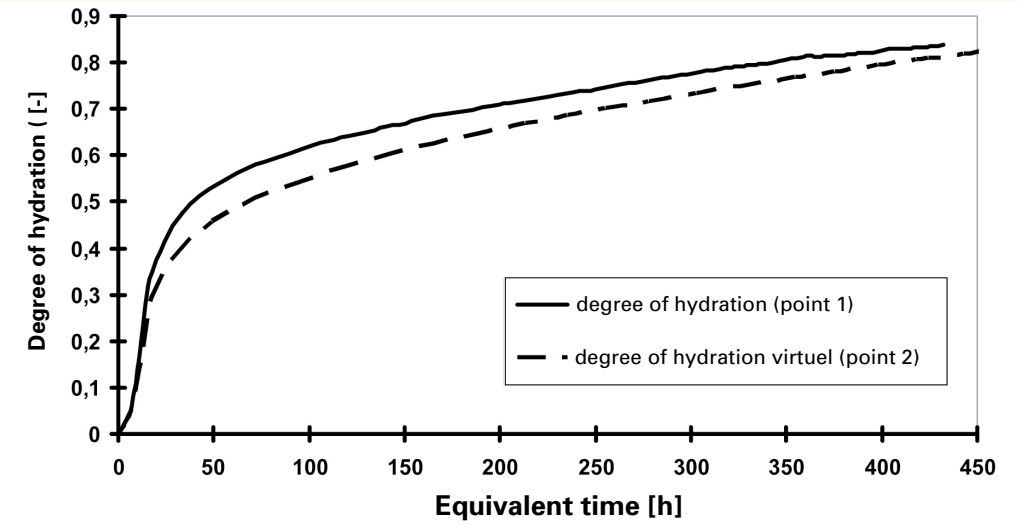

Figure 13
Losses vs. temperature difference

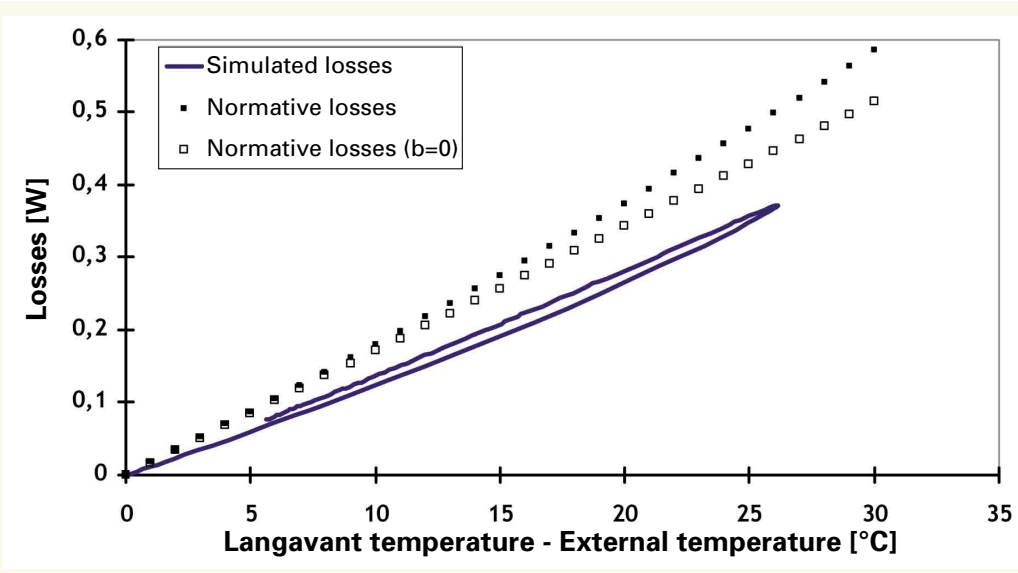

INFLUENCE OF ACTIVATION ENERGY

As previously observed, cement activation energy is necessary during analysis of the QAB test in order to determine the evolution in degree of hydration vs. temperature. Furthermore, this energy is involved in the chemical affinity calculation (which is also determined based on calorimetric test results), according to the relation set forth in **(3)**.

In a thermal simulation, this parameter appears twice. The first time is explicit when calculating the degree of hydration, and the second is implicit when expressing chemical affinity. Our goal therefore was to identify, by a numerical study, the influence that this parameter was capable of exerting on temperature evolution inside a massive structure. To proceed, we relied upon a simple geometry representing a wall poured onto a raft foundation and then simulated the changes in wall temperature at the level of the various probes during the hydration phase. Both the wall dimensions and probe positions are given in **Figure 14**. The evolution in adiabatic temperature is derived from a QAB type of semi-adiabatic test.

Let's restate our preference for using a constant value of activation energy, as Broda *et al.* **[4]** had demonstrated that activation energy depended on temperature (e.g. [Grube], as cited in Springerschmidt **[19]**); these authors also concluded that a single apparent activation energy would suffice. This result was confirmed by Xiong and Van Breugel **[22]**. Let's also recall however that this process involves a macroscopic apparent activation energy since in reality, each phase of cement is associated with its own activation energy **[2, 17]**.

As a next step, we covered a wide range of activation energy values, extending from E_a/R = 4,000 K to E_a/R = 7,000 K. The results of this parametric study are presented in **Figure 15**. It should be noted that for each activation energy value, we recalculated the evolution in chemical affinity as well (**Equation 3**).

The results of these simulations highlight the limited influence of activation energy not only on the maximum temperature obtained for each probe, but also on the temperature evolution kinetics, which might seem even more surprising. This finding is explained by the fact that chemical affinity calculated from the activation energy considered as well as from the calorimetric test actually has a compensating effect on the activation energy value: it is necessary therefore to include the couple $(\tilde{A}(\xi), E_a/R)$.

Moreover, this study demonstrates that an approximate value of activation energy (e.g. calculated from both the chemical composition of cement and values provided by Kishi *et al.* **[14],** as cited in

Figure 14
Dimensions of the modeled wall and thermal probe positions

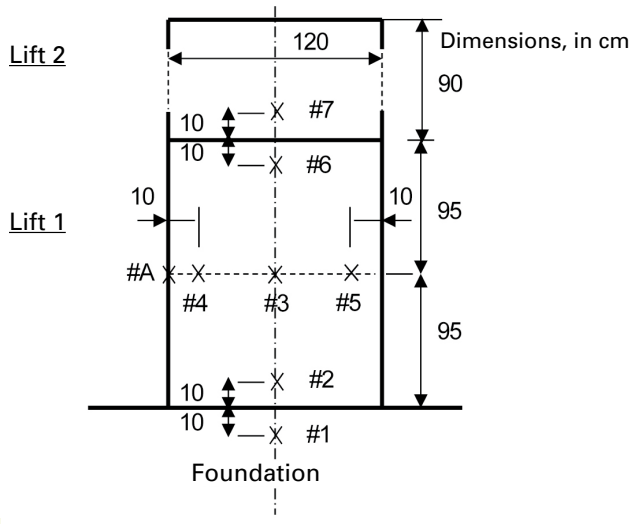

Figure 15
Temporal evolution of temperature calculated inside the wall

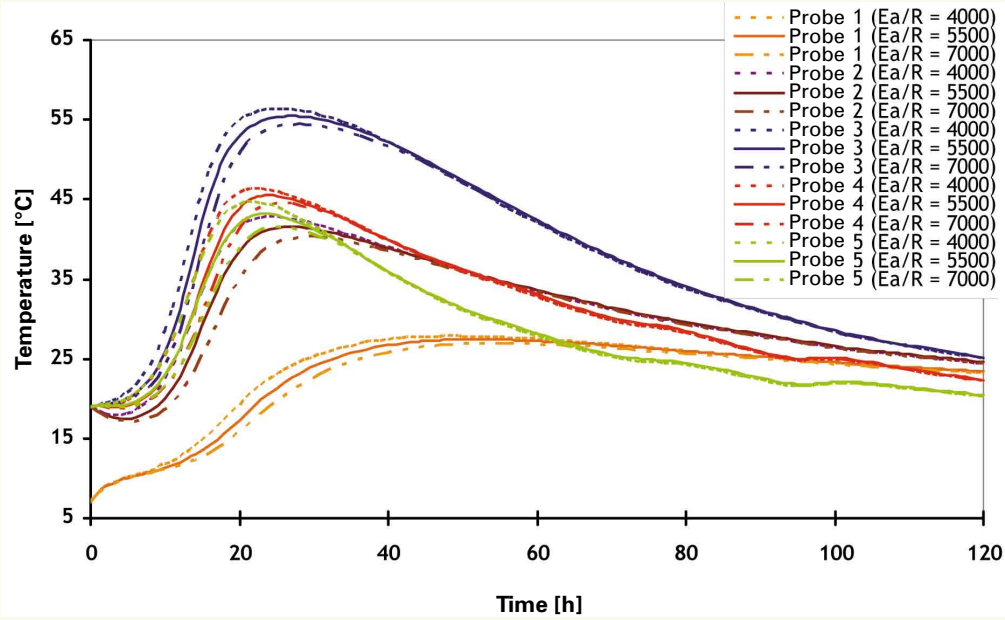

[5]) is sufficient to predict temperature evolution in a massive structural element, meaning that a semi-adiabatic calorimetric test is by itself sufficient.

CONCLUSION

The simulations of both QAB and Langavant type calorimetric tests have enabled validating a number of hypotheses adopted during test execution, in addition to rejecting a number of test protocol simplifications through the quantification of errors committed:

• Though calorimeters are calibrated in the steady state whereas the test is conducted in a transient state, the form of the equation that quantifies heat losses may be set up as a linear function (i.e. $y = \alpha.(\theta)\theta$, with $\alpha(\theta) = a + b\theta$, and b having a small value).

• For the QAB test, heat accumulated in the insulating material can be neglected. The proposed analytical equation **(1)**, which integrates the accumulated heat and losses, is thus justified by the numerical simulations performed.

• Despite the established preference for a QAB type calorimeter when testing a material like concrete, the use of an ECM and Langavant type calorimeter also allows determining the chemical affinity and latent heat of hydration of the reference concrete.

• Unprecise thermal probe placement (outside the sample) during a Langavant test introduces a significant error on the latent heat of hydration value, along with a separate error on the evolution in degree of hydration. Centimeter-level accuracy is all that's required when positioning the temperature probe inside the sample for both types of tests.

Lastly, a parametric study of the influence of activation energy has underscored the potential for using an approximate value of this energy provided the couple ($\tilde{A}(\xi)$, E_a/R) has been introduced into the numerical simulation. A precise experimental determination of activation energy imposes conducting two semi-adiabatic tests in two distinct environments (e.g. 2 different external temperatures), which necessitates appropriate testing equipment and thereby increases the costs associated with this type of test. The results obtained from this study would indicate that a single test is sufficient to accurately predict temperature evolution within a massive structural element.

RÉFÉRENCES BIBLIOGRAPHIQUES

1 **Acker P.**, "Thermal effect in concrete during manufacture and applications to engineering structures", *Annales de l'Institut Technique du Bâtiment et des Travaux Publics* N° 442, **February 1986**, pp. 61-80

2 **Ballim Y.**, **Graham P.C.**, "Early age heat evolution of clinker cements in relation to microstructure and composition : implications for temperature development in large concrete elements", *Cement & Concrete Composites* Vol. 26, Issue 5, **July 2004**, pp. 417-426

3 **Bamforth P.B.**, "In-situ measurement of the effect of partial Portland cement replacement using either fly ash or ground granulated blast-furnace slag on the early age behaviour of mass concrete", *Taylor Woodrow Reasearch Projet* N°014J/77/1939, **Nov 1977**, p. 104

4 **Broda M.**, **Wirquin E.**, **Duthoit B.**, "Conception of an isothermal calorimeter for concrete – determination of the apparent activation energy", *Materials and structures* N°35, **2002**, pp. 389-394

5 **Buffo Lacarrière L.**, "Prévision et évaluation de la fissuration précoce des ouvrages en béton", Thèse de l'université de Toulouse (LMDC), **2007**

6 **Clément J.L.,** "Exemple de calcul en Europe", In : *"Comportement du béton au jeune âge"* (Traité MIM, série Matériaux de construction), Acker Paul, Torrenti Jean-Michel, Ulm Franz-Josef, eds, **2004**, 188 pages

7 **Coole M.J.**, "Heat release caracteristics of concrete containing ground granulated blastfurnace slag in simulated large pours", *Magazine Concrete Research 40*, N°144, **Sept 1988**, pp. 152-158

8 Commissariat à l'énergie atomique (CEA) DEN/DM2S/SEMT, Code éléments finis Cast3m, disponible sur http://www-cast3m.cea.fr/

9 **Costa U.**, "A simplified model of adiabatic calorimeter", *Il Cemento* 76, N°2, **April 1979**, pp. 75-92

10 **D'Aloïa L.**, **Chanvillard G**, "Determining the ''apparent'' activation energy of concrete Ea – Numerical simulations of the heat of hydration of cement", *Cement and Concrete Research* 32(8), **2002**, 1277-1289

11 EN 196-9, "Méthode d'essais des ciments – Chaleur d'hydratation – Méthode semi-adiabatique", *Norme Européenne* NFEN 196-9, **2004**

12 **Freiesleben Hansen P.**, **Pedersen E.J.**, "Maturity computer for controlled curing and hardening of concrete", *Nordic Concrete Research*, vol. 1, **1977**, pp. 21–25

13 **Hernot H.**, **Porcher G.**, *"Thermique appliquée aux bâtiments"*, Éditions parisiennes, **1984**, ISBN 2862430153

14 **Kishi T.**, **Maekawa K.**, "Thermal and mechanical modelling of young concrete based on hydration process of multi-component cement materials", *Thermal cracking in concrete at early age, Rilem Proceeding* 25, **1994**, ISBN 0-419-18710-3, pp. 11-19

15 **Mounanga P.**, **Khelidj A.**, **Bastian G.**, "Experimental studies and modelling approaches for the thermal conductivity evolution of hydrating cement paste", *Advances in Cement Research*, 16, n° 3, **2004**, pp. 95-103

16 **Regourd M.**, **Gauthier E.**, "Comportement des ciments soumis à un durcissement accéléré", *Annales de l'ITBTP* 179, **1980**, pp. 65-96

17 **Schindler A.K.**, "Effect of temperature on hydration of cementitious materials", *ACI Mat. J.* 101(1), **2004**, pp. 72-81

18 **Schwartzentruber A.**, **Catherine C**, "La méthode du mortier de béton équivalent (MBE). Un nouvel outil d'aide à la formulation des bétons adjuvantés", *Materials and Structures* 33, **2000**, pp. 475-482

19 **Springenschmidt, R.** (Ed.), Prevention of Thermal Cracking in Concrete at Early Ages – State of the Art Report. London: E&FN Spon, **1998**

20 **Suzuki Y.**, "Evaluation of adiabatic temperature rise of concrete measured with the new testing apparatus", *Concrete library of JSCE*, N°13, **June 1989**

21 **Ulm F.J.**, **Coussy O.**, "Couplings in early-age concrete : from material modelling to structural design", *International Journal of Solids and Structures* 35(31-32), **1998**, pp. 4295-4311

22 **Waller V.**, "Relations entre composition des bétons, exothermie en cours de prise et résistance en compression", *Collection Études et Recherches des laboratoires des Ponts et Chaussées* – série Ouvrages d'Art OA35 – LCPC, **2000**

23 **Xiong X.**, **Van Breugel K.**, "Isothermal calorimetry study of blended cements and its application in numerical simulations", *Heron* **2001** Références bibliographiques